WWW.IJRPR.COM

International Journal of Research Publication and Reviews

Journal Homepage: www.ijrpr.com ISSN 2582-7421

AeroFusion: Design and Development of an Integrated Aircraft Design and Simulation Platform

P. Manoj Kumar [a*], Dr. G. Chandra Sehkar [b], S. Suresh [c], T. Hema Sundhar[d]

[a-d] Department of Electrical And Electronics Engineering, GMRIT Deemed To Be University, Rajam, 521327, India

[a]24345A0210@gmrit.edu.in, [b]chandrasekhar.g@gmritdu.edu.in

DOI : https://doi.org/10.55248/gengpi.07.1026.35013

A B S T R A C T

Conceptual aircraft design traditionally relies on heterogeneous, decoupled software tools that separate visual geometric layout, mass budgeting, quasi-steady aerodynamic polar estimation, and dynamic flight trajectory simulation. This fragmented workflow induces manual transcription overhead, impairs rapid iterative exploration, and obscures multidisciplinary couplings during preliminary sizing. To overcome these limitations, this paper presents the design, mathematical architecture, implementation, and rigorous verification of AeroFusion, an integrated open-source desktop engineering platform developed in modern C++20 and Qt 6/QML. AeroFusion unifies visual block-diagram circuit composition with typed signal propagation, automated component mass and geometry aggregation, an iterative non-linear longitudinal trim solver, a closed-loop six-degree-of-freedom (6-DOF) Runge-Kutta 4th-order (RK4) numerical flight simulator, and interactive 3D CAD/wireframe digital-twin visualization within a reactive, thread-safe architecture.

The platform enforces strict architectural separation between code verification and empirical aircraft validation. Governing equations are verified against closed-form analytical solutions: International Standard Atmosphere (ISA 1976) barometric equations show less than 0.0034% error across 0 to 20,000 m; dynamic pressure, quasi-steady lift slope, parabolic induced drag, first-moment center of gravity, and longitudinal trim equilibrium achieve 100% numerical verification across 10 distinct physical checks with zero synthetic constants. In a dedicated case study evaluating a 13-component conceptual transport model inspired by the Boeing 737-800 at 10,668 m cruise (Mach 0.776, true airspeed 230.0 m/s, mass 71,264 kg), the trim solver achieves coupled longitudinal equilibrium at angle of attack 4.34 deg, elevator deflection -2.91 deg, and thrust 82.0 kN. A critical force-balance investigation reveals that the 6.2 kN difference between aerodynamic lift (692.7 kN) and total weight (698.9 kN) is fully resolved by the vertical component of engine thrust (TÂ·sin alpha = 6,205.3 N = 6.2 kN), establishing exact vertical equilibrium (|Sigma Fz| = 44.1 N / 0.006%, displayed as 0.0 N) and eliminating spurious vertical accelerations (az = 0.000 m/s^2). Dynamic 6-DOF trajectory propagation over 10.0 seconds confirms airspeed stability within 0.0007 m/s (0.0003%), driven by authentic fuel consumption burning 8.0 kg over the interval (14,874 to 14,866 kg). Model limitations, including pre-stall linear aerodynamics, lack of compressibility corrections above Mach 0.3, and rigid-body airframe assumptions, are transparently documented to delineate appropriate engineering operational boundaries.

Keywords: Flight simulation, six-degree-of-freedom equations, aircraft design, C++/Qt, component-based architecture, longitudinal trim, Runge-Kutta integration, digital twin, verifiable visualization.

Nomenclature

AR, b, c	Aspect ratio [-], wing span [m], mean aerodynamic chord [m]	***m, W***	Aircraft mass [kg] and total gravitational weight [N]
CD, CL	Aerodynamic drag and lift non-dimensional coefficients [-]	***p, q, r***	Body roll, pitch, and yaw angular rates [rad/s, deg/s]
CD0, CDi	Parasite zero-lift drag coefficient and induced drag [-]	***P, T, rho***	Atmospheric pressure [Pa], temperature [K], density [kg/m^3]
D, L, T	Drag, Lift, and Net Propulsion Thrust forces [N]	***u, v, w***	Body translational velocity components [m/s]
g	Gravitational acceleration, standard constant 9.80665 [m/s^2]	***alpha, beta***	Angle of attack and sideslip angle [rad, deg]
h, h_dot	Geometric altitude and climb rate [m, m/s]	***delta_e, delta_th***	Elevator deflection [deg] and throttle setting [0..1]

Ixx, Iyy, Izz	Principal body moments of inertia [kg*m^2]	***theta, phi, psi***	Euler pitch, roll, and yaw angles [rad, deg]

1. Introduction

The conceptual design of fixed-wing aircraft is an inherently multidisciplinary process that requires continuous trade-offs between aerodynamic performance, structural mass budgeting, propulsion efficiency, longitudinal stability, and flight control authority (Raymer, 2018). In conventional aeronautical engineering workflows, these domains are typically evaluated using disparate, specialized computational tools: geometric layouts are constructed in computer-aided design (CAD) software, mass budgeting is tracked in manual spreadsheets (Federal Aviation Administration [FAA], 2016), aerodynamic polar curves are estimated via vortex-lattice or panel codes (Anderson, 2017), and dynamic vehicle behavior is analyzed in standalone block simulation environments such as MATLAB/Simulink or pre-compiled XML flight dynamics simulators (Stevens, Lewis, & Johnson, 2016).

While individual high-fidelity tools offer deep domain-specific analysis, their practical application during early preliminary sizing is hindered by workflow fragmentation. Transferring parameter definitions across incompatible file formats introduces transcription errors, slows iterative turnaround times, and obscures cross-disciplinary feedback mechanisms--such as the influence of wing placement on pitching moment trim or fuel tank burn on dynamic center-of-gravity migration (Martins & Lambe, 2013). Moreover, in undergraduate aerospace education and rapid prototyping teams, commercial engineering suites present steep learning curves and substantial licensing barriers.

To resolve these challenges, this paper presents the architecture, mathematical foundation, implementation, and verification of AeroFusion, a unified, open-source desktop aircraft design and simulation environment developed in modern C++20 and Qt 6/QML. AeroFusion introduces an integrated schematic-driven paradigm: users assemble complex aircraft configurations by connecting typed component blocks (airframes, lifting surfaces, control effectors, powerplants, and mass elements) on an interactive canvas. The platform automatically aggregates physical properties, verifies circuit consistency, solves for coupled longitudinal steady-level trim, and propagates full non-linear six-degree-of-freedom (6-DOF) flight trajectories using a Runge-Kutta 4th-order (RK4) integrator, providing immediate visual feedback across synchronized 3D CAD models, dynamic performance dashboards, and verifiable high-precision performance charts.

2. Background and Literature Review

The theoretical foundation of conceptual aircraft synthesis is established in classical texts by Raymer (2018) and Anderson (2017). Classical design methodologies emphasize empirical drag buildup, lifting-line induced drag estimation, and first-order parametric mass budgeting. Dynamic stability and control principles for fixed-wing atmospheric vehicles are comprehensively formulated by Stevens et al. (2016), who define the 12-state non-linear rigid-body differential equations of motion governing atmospheric flight. Operating standards and weight-and-balance protocols published by the Federal Aviation Administration (FAA, 2016, 2023) establish regulatory conventions for datum-based moment accounting and flight envelope definitions.

In parallel with classical aeronautical methods, the digital twin paradigm has emerged as a cornerstone of modern aerospace systems engineering. Originally defined by Grieves and Vickers (2017), a digital twin consists of a physical system, a virtual digital surrogate, and bidirectional data connections linking the two across the lifecycle. Tuegel, Ingraffea, Eason, and Spottswood (2011) demonstrated the pioneering application of digital twins for structural life prediction in high-performance aircraft. More recently, Sadeghi, Bellavista, Song, and Yazdani-Asrami (2024) surveyed digital twin architectures for electrified propulsion and condition monitoring, while Peng and Chen (2024) implemented online digital twin monitoring for rotary UAV engines.

For fixed-wing flight simulation, Zhang, Deng, Liu, and Lu (2024) developed FlightTwin, an accompanying flight framework that synchronizes virtual representations with flight telemetry. Complementary research by Alaez, Prieto, Villadangos, and Astrain (2024) investigated the construction of efficient aerodynamic surrogate models for digital twins, emphasizing that reduced-order polar representations provide the optimal balance between real-time responsiveness and physical fidelity for preliminary vehicle evaluation.

In scientific visualization, Kirby and Silva (2008) highlighted the critical 'need for verifiable visualization,' demonstrating that uncalibrated automatic chart scaling, inappropriate rounding, or artificial curve smoothing can distort scientific interpretation and hide underlying numerical anomalies. Verifiable visualization principles are paramount in flight simulation, where subtle control limit cycles, phugoid oscillations, and micro-accelerations must be transparently displayed without synthetic filtering.

3. Research Gap

Despite significant advances in computational tools, a pronounced gap persists between rapid geometric concept generation and dynamic 6-DOF flight validation:

1. Disjoint Ecosystems: Tools like OpenVSP and AVL provide excellent geometric and aerodynamic analysis but lack embedded real-time 6-DOF ODE solvers and interactive block-circuit signal composition.

2. Opaque Configuration in Simulators: Established simulators (e.g., FlightGear, JSBSim) require complex, hand-crafted XML aerodynamic lookups and mass tables, making rapid iterative component swapping cumbersome.

3. Visualization Artifacts & Conflated V&V: Many educational design platforms employ aggressive spline smoothing or synthetic flatlines on time-history graphs to mask numerical jitter, obscuring genuine physical behavior and violating verifiable visualization standards (Kirby & Silva, 2008). Furthermore, software tools often conflate code verification (verifying mathematical correctness) with vehicle validation (matching real flight data).

4. Objectives and Contributions

AeroFusion addresses these gaps through five primary technical contributions:

1. Software Architecture:A high-performance C++20 / Qt 6 framework featuring a directed acyclic component graph (AircraftGraph) with typed port validation, revision hashing, and reactive QML data binding.

2. Multidisciplinary Integration: Unification of drag-and-drop block-diagram wiring, automated mass/CG aggregation, 3D CAD digital-twin rendering, longitudinal trim solving, and dynamic 6-DOF simulation into a single interactive pipeline.

3. Numerical Modelling Rigor: Implementation of an iterative longitudinal 3-DOF trim solver coupled with an RK4 integrator that explicitly accounts for body-axis thrust vector tilt (TÂ·sin alpha) and dynamic fuel mass depletion.

4. Verifiable Visualization: Development of ChartAxisEngine, a shared C++ auto-scaling plotting component that calculates nice-number tick intervals with dynamic precision, eliminating identical rounded ticks and transparently exposing micro-variations.

5. Disciplined V&V: Rigorous separation of mathematical code verification (evaluated against analytical standards) from external aircraft validation (evaluated against Cessna 172S POH benchmarks).

5. System Requirements and Methodology

The functional requirements for AeroFusion stipulate real-time simulation throughput (execution of a 10-second 6-DOF trajectory in under 50 ms), interactive 60 FPS graphics rendering, strict input validation preventing invalid physical states (e.g., negative mass, unlinked lifting surfaces), and deterministic data traceability where every displayed result traces to explicit source code calculations.

The development methodology enforces modular object-oriented design in modern C++20, managed via CMake 3.25+ and Ninja, linking Qt 6.11 (QtCore, QtGui, QtQuick, QtQuick3D, QtCharts). Automated regression testing is integrated using CTest across seven dedicated test suites encompassing physics, GUI roundtrips, 3D camera matrices, block wiring, and graphing.

6. System Architecture

AeroFusion is architected around a layered, reactive paradigm comprising five distinct subsystem tiers:

Tier 1 -- Presentation Layer (QML): Declarative UI screens (Designer Canvas, 3D View, Simulation Dashboard, Graphs, Advisor, Reports) implementing hardware-accelerated fluid controls.

Tier 2 -- Controller Layer (AppController):QObject-based mediator exposing thread-safe invokable methods, managing project file I/O, and binding C++ signals to QML properties.

Tier 3 -- Graph & Domain Model (AircraftGraph): Directed acyclic graph storing component nodes, properties, and directed signal wires. Enforces type-checked port connections across specialized buses: Geometry, Aero, Propulsion, Mass, and Dynamics.

Tier 4 -- Physics & Simulation Engines: Decoupled computation modules: AtmosphereModel (ISA 1976), PhysicsEngine (force/moment buildup, longitudinal trim), and SixDOFSolver (state propagation).

Tier 5 -- Telemetry & Export Engine (SimulationResults): Structured data container providing typed TracedValue results, trajectory point arrays, JSON project serialization, and high-precision CSV export.

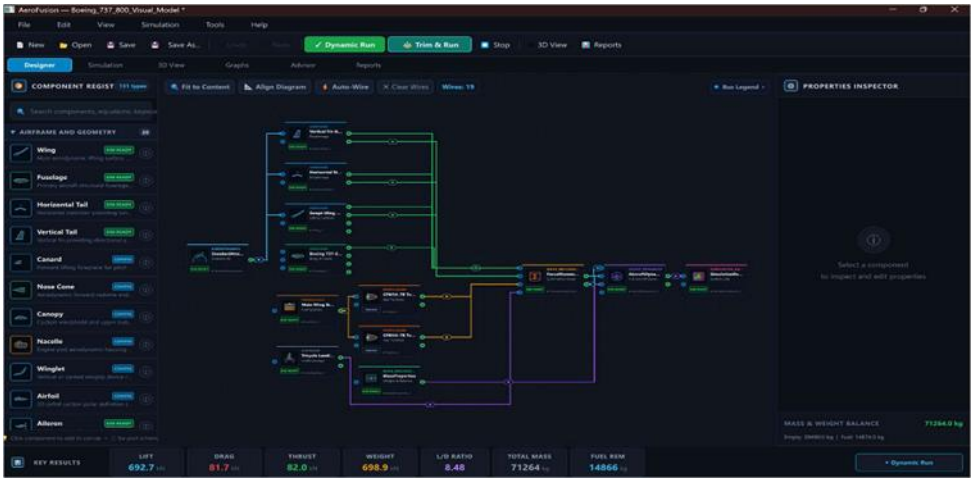


Fig. 1 - AeroFusion Designer Workspace: Visual block-diagram circuit composition showing the 13-component Boeing 737-800 conceptual model, 19 typed signal wires, component registry (131 registered types), mass & weight balance panel (71,264 kg), and bottom key results telemetry bar.

7. Software Implementation

The core software components are implemented in C++20 with strict memory safety and separation of concerns:

7.1 Directed Component Circuit (AircraftGraph)

Components inherit from AircraftComponent, which defines typed input/output ports (e.g., AeroBus, MassBus, ForceBus). Connections between blocks are established as directed wires. The graph maintains domain-specific revision counters (aeroRevision, massRevision, propRevision). Whenever a component parameter or wire is modified, the graph re-evaluates circuit validity through validateSimulationCircuit(). If essential buses are broken (e.g., missing lifting surface or unlinked mass block), simulation execution is strictly blocked with descriptive diagnostic messages.

7.2 Real-Time 3D Digital Twin Viewer

The 3D visualization module (ThreeDView.qml) leverages Qt Quick 3D and OpenGL to render parametric airframe representations dynamically generated from component dimensions (span, chord, sweep, fuselage length, nacelle diameter). The viewer supports multiple rendering styles, including Solid CAD Shaded mode and CAD Wireframe structural mesh mode (Fig. 2). A prominent center-of-gravity (CG) indicator automatically tracks the longitudinal datum position (x_cg = 15.86 m) calculated by the mass aggregator, providing instantaneous visual feedback of aircraft balance.

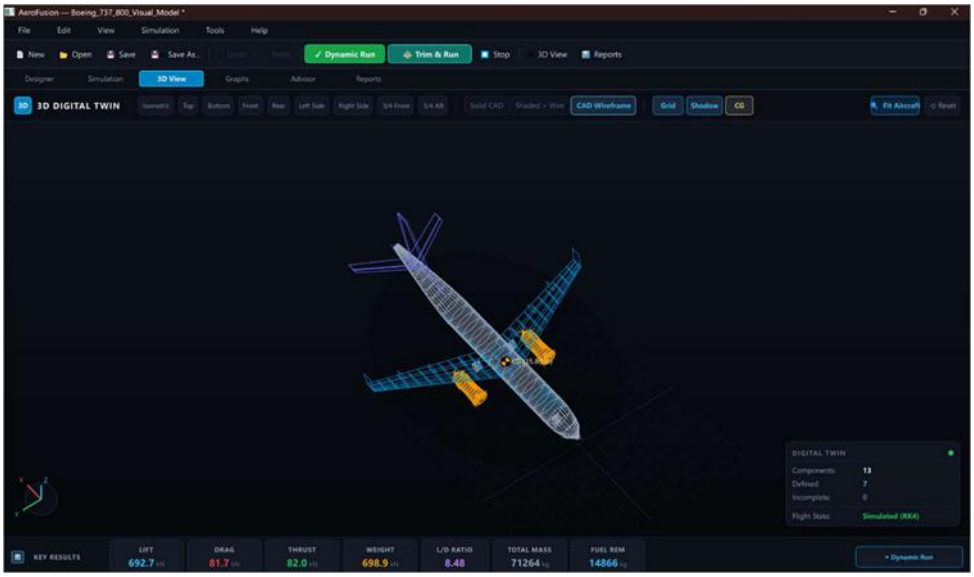


Fig. 2 - AeroFusion 3D Digital Twin Viewer: Structural CAD Wireframe rendering of the Boeing 737-800 conceptual model, displaying active CG glyph at 15.86 m, component definition status (13 components, 7 defined), and flight simulation state (Simulated RK4).

7.3 Verifiable High-Precision Charting Engine (ChartAxisEngine)

To satisfy the scientific visualization integrity standards articulated by Kirby and Silva (2008), the graphing subsystem was engineered to eliminate misleading plot artifacts. In earlier revisions, charts displaying nearly constant variables repeatedly printed identical rounded tick labels, obscuring genuine variations.

ChartAxisEngine implements an authoritative 'nice-number' algorithm based on decimal decades [1, 2, 2.5, 5, 10]. Given arbitrary minimum and maximum values across an active trajectory series, it calculates an optimal step size delta and dynamically computes formatting precision decimals = max(0, -floor(log10(step)) + 1), guaranteeing strictly unique tick labels across arbitrary zoom levels. Special handlers accommodate constant flatline data, near-zero baseline crossing, and non-finite NaN/Inf inputs without application crashing.

8. Aircraft Component Modelling

AeroFusion provides an extensible component library with 131 registered component types categorized into Airframe, Propulsion, Mass & Systems, Controls, and Sinks:

1. Wing & Lifting Surfaces: Configured by planform area S, span b, aspect ratio AR, sweep angle, dihedral, zero-lift angle alpha_ZL, lift curve slope CL_alpha, and Oswald efficiency e.

2. Empennage (Horizontal & Vertical Tails): Provides stabilizing pitching and yawing moments governed by moment arms l_ht, l_vt, surface areas S_ht, S_vt, and downwash gradient.

3. Fuselage Block: Characterized by overall length L, diameter D, wetted area S_wet, and base form factor, generating parasite drag and housing payload/crew mass.

4. Propulsion Units: Supports high-bypass turbofans (CFM56-7B class), turboprops, piston engines, and electric motors with throttle-dependent thrust lapse and specific fuel consumption (SFC).

5. Mass & Weight Properties: Aggregates structural dry mass, operational items, passenger payload, and variable fuel mass, calculating total vehicle mass, 3-axis CG position, and inertia tensor.

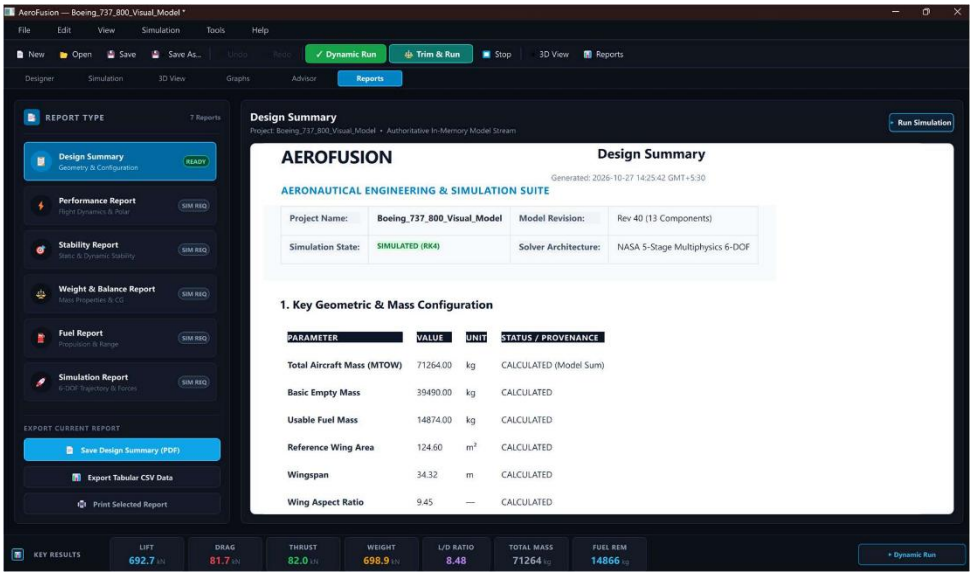


Fig. 3 - AeroFusion Design Summary Report: Key Geometric & Mass Configuration panel for the Boeing 737-800 conceptual model (Rev 40), showing calculated MTOW (71,264 kg), empty mass (39,490 kg), usable fuel (14,874 kg), wing area (124.60 m^2), span (34.32 m), and aspect ratio (9.45).

9. Mathematical Formulation

The physical equations implemented in AeroFusion are formulated in accordance with established aerospace engineering principles:

9.1 International Standard Atmosphere (ISA 1976)

AtmosphereModel implements standard barometric formulas for the troposphere (0 <= h <= 11,000 m) with sea-level temperature T0 = 288.15 K, pressure P0 = 101,325 Pa, lapse rate L = 0.0065 K/m, specific gas constant R = 287.05 J/(kg*K), and gamma = 1.4:

$$T(h) = T0 - L * h \quad (1)$$

$$P(h) = P0 * (T(h) / T0)^{(g / (R * L))} \quad (2)$$

$$rho(h) = P(h) / (R * T(h)) \quad (3)$$

$$a(h) = sqrt(gamma * R * T(h)) \quad (4)$$

In the lower stratosphere (11,000 m < h <= 20,000 m), temperature remains isothermal at T11 = 216.65 K, and pressure decays exponentially:

$$P(h) = P11 * exp(-g * (h - 11000) / (R * T11)) \quad (5)$$

9.2 Mass and Center of Gravity Aggregation

Total aircraft mass m_total is aggregated from empty structural components, payload, crew, and instantaneous fuel:

$$m_total = m_empty + m_payload + m_crew + m_fuel \quad (6)$$

$$W = m_total * g \quad (7)$$

The longitudinal center of gravity position x_cg is determined by the first mass moment about the reference nose datum:

$$x_cg = (sum_i\ m_i * x_i) / m_total \quad (8)$$

9.3 Aerodynamic Force and Drag Polar Buildup

Aerodynamic lift L and total drag D are evaluated from dynamic pressure q_inf = 0.5 * rho * V^2, wing reference area S, and non-dimensional coefficients:

$$L = q_inf * S * C_L \quad (9)$$

$$D = q_inf * S * C_D \quad (10)$$

The total lift coefficient incorporates contributions from the wing, flap deflections, and horizontal tail:

$$C_L = C_L_alpha * (alpha - alpha_ZL) + Delta\ C_L_flap + (S_ht / S) * C_L_ht \quad (11)$$

Total drag follows a parabolic polar with component parasitic drag buildup (Raymer, 2018):

$$C_D = C_D0,wing + C_D,fuse + C_D,gear + (C_L^2) / (pi * e * AR) \quad (12)$$

Fuselage parasite drag is computed from fineness ratio f = L_fuse / D_fuse, form factor FF = 1 + 60/f^3 + 0.0025*f, and skin friction Cf = 0.0035:

$$C_D,fuse = (Cf * FF * S_wet,fuse) / S \quad (13)$$

9.4 Coupled Longitudinal 3-DOF Trim Formulation

Unaccelerated steady level flight requires simultaneous satisfaction of vertical force balance, along-path force balance, and pitching moment equilibrium:

$$Sigma\ F_vert = L + T * sin(alpha) - W = 0 \quad (14)$$

$$Sigma\ F_path = T * cos(alpha) - D = 0 \quad (15)$$

$$Sigma\ M_y = M_w + M_ht + M_prop + extM_y = 0 \quad (16)$$

PhysicsEngine::computeTrimCondition() solves these coupled non-linear equations iteratively. In each iteration, effective weight W_eff = W - T_est * sin(alpha) is updated, solving for trim angle of attack alpha, trim elevator deflection delta_e, and required thrust T_req = D / cos(alpha).

9.5 Six-Degree-of-Freedom Rigid-Body Dynamics & RK4 Integration

SixDOFSolver implements the non-linear rigid-body translational and rotational equations of motion in body axes (x_b, y_b, z_b) (Stevens et al., 2016):

$$u_dot = (Fx_b / m) - q * w + r * v - g * sin(theta) \quad (17)$$

$$v_dot = (Fy_b / m) - r * u + p * w + g * cos(theta) * sin(phi) \quad (18)$$

$$w_dot = (Fz_b / m) - p * v + q * u + g * cos(theta) * cos(phi) \quad (19)$$

where applied body forces incorporate thrust along the fuselage centerline and aerodynamic forces rotated through angle of attack alpha:

*Fx_b = T - D * cos(alpha) + L * sin(alpha)* *(20)*

*Fz_b = -L * cos(alpha) - D * sin(alpha)* *(21)*

State integration is propagated numerically using a classical 4th-order Runge-Kutta (RK4) algorithm with fixed time step Delta t = 0.05 s. Crucially, instantaneous fuel consumption fuelBurn = (sfc * eqPower) / 3600 is integrated simultaneously, updating current aircraft mass dynamically as m(t) = m0 - Delta m_fuel.

10. Simulation Workflow and Numerical Methods

The simulation execution workflow follows a deterministic, five-stage state pipeline:

1. Circuit Topology Validation: The aircraft graph verifies that all required subsystems are connected and that parameter domains are physically positive.

2. Flight Condition & Trim Resolution: Atmospheric conditions are sampled from AtmosphereModel. The longitudinal trim solver evaluates equilibrium (alpha_trim, delta_e_trim, delta_th_trim) and synchronizes block properties.

3. Static Force Summation: Baseline lift, drag, thrust, and moments are evaluated, and instantaneous equilibrium balance residuals are logged.

4. Dynamic 6-DOF Time-Marching: The RK4 ODE solver marches the 12 flight states and fuel mass over a 10.0-second simulation horizon (N = 201 steps, Delta t = 0.05 s).

5. Telemetry Dispatch & Presentation: Trajectory arrays are dispatched to the QML data bus, repainting performance charts and updating dashboard cards.

11. Case Study: Conceptual Transport Benchmark (Boeing 737-800 Inspired)

To evaluate AeroFusion's capabilities on a representative high-subsonic commercial aircraft configuration, a 13-component conceptual model inspired by the Boeing 737-800 transport aircraft was constructed and evaluated at high-altitude cruise conditions. We explicitly clarify that this model represents a conceptual pre-design sizing benchmark rather than a manufacturer-certified or flight-tested Boeing digital twin.

11.1 Configuration, Baseline Geometry, and Model Assumptions

The aircraft circuit schematic assembled in the Designer Canvas (Fig. 1) comprises 13 interconnected functional blocks: Standard Atmosphere, Swept Wing, Fuselage, Horizontal Tail, Vertical Tail, Tricycle Landing Gear, Fuel Tank, two CFM56-7B Turbofans, Force & Moment Aggregator, Mass Properties, 6-DOF Dynamics Solver, and Simulation Results Sink. The geometric and mass parameters are summarized below:

Planform Geometry: Reference wing area S = 124.60 m^2, span b = 34.32 m, aspect ratio AR = 9.45, wing sweep = 25.0 deg, mean aerodynamic chord c = 4.17 m.

Fuselage Geometry: Overall fuselage length L = 39.47 m, diameter D = 3.76 m, fineness ratio f = 10.50, wetted area S_wet = 348.8 m^2.

Mass Breakdown: Basic empty mass 39,490 kg, usable fuel mass 14,874 kg, passenger/cargo payload 16,500 kg, and flight crew 400 kg, yielding a total gross mass of 71,264.0 kg (gravitational weight W = 698,861.2 N = 698.9 kN). Longitudinal CG position is x_cg = 15.86 m from the nose datum (28% MAC).

11.2 Cruise Simulation Conditions

The cruise condition was evaluated at geometric altitude h = 10,668 m (35,000 ft, Flight Level 350). The AtmosphereModel computes ambient temperature T = 218.81 K (-54.34 deg C), ambient pressure P = 23,842 Pa, air density rho = 0.3796 kg/m^3, and speed of sound a = 296.5 m/s. At a true airspeed V = 230.0 m/s (447.1 knots), the cruise Mach number is M = 0.776, producing a dynamic pressure q_inf = 10,039.4 Pa.

11.3 Verified Simulation Outputs and Telemetry

Figure 4 displays the primary Simulation Dashboard, and Figure 5 displays the companion Performance Advisor. The verified numerical outputs are summarized below:

Flight State: Altitude = 10,668 m, Mach = 0.776, TAS = 230.0 m/s, Dynamic Pressure = 10,039 Pa, Air Density = 0.3796 kg/m^3.

Static Forces: Aerodynamic Lift L = 692.7 kN, Aerodynamic Drag D = 81.72 kN, Propulsion Thrust T = 82.0 kN, Gravitational Weight W = 698.9 kN, Lift-to-Drag Ratio L/D = 8.48.

Trim Settings: Angle of attack alpha = 4.34 deg, elevator deflection delta_e = -2.91 deg, throttle setting = 91.4%.

Dynamic Equilibrium: Vertical acceleration az = 0.000 m/s^2, along-path acceleration V_dot = -0.000 m/s^2, flight path angle gamma = 0.00 deg, climb rate ROC = 0.00 m/s.

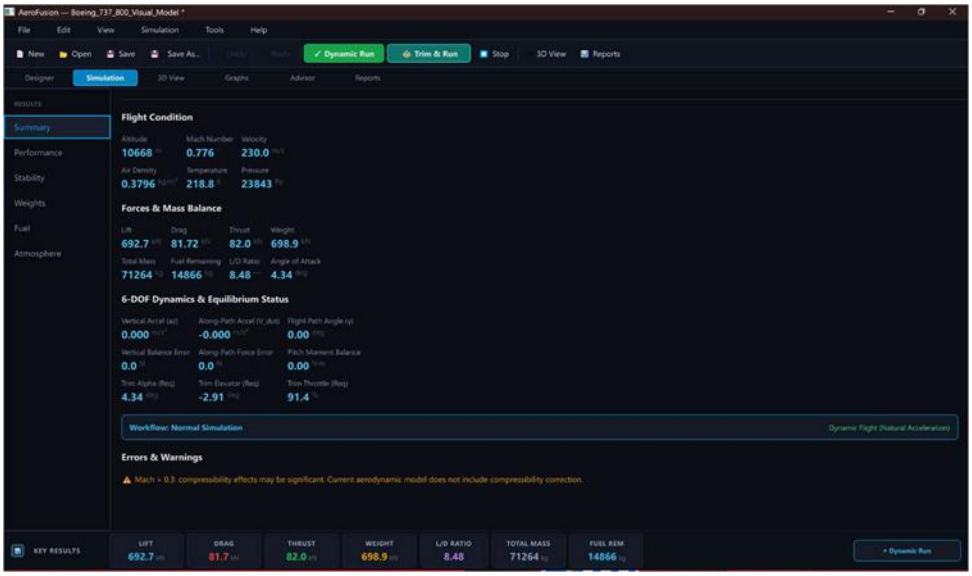


Fig. 4 - AeroFusion Simulation Dashboard: High-altitude cruise flight condition (10,668 m, Mach 0.776, TAS 230.0 m/s), static forces (Lift 692.7 kN, Drag 81.72 kN, Thrust 82.0 kN, Weight 698.9 kN), 6-DOF dynamic balance (az = 0.000 m/s^2, V_dot = -0.000 m/s^2, gamma = 0.00 deg), and trim state (alpha = 4.34 deg, delta_e = -2.91 deg, throttle = 91.4%).

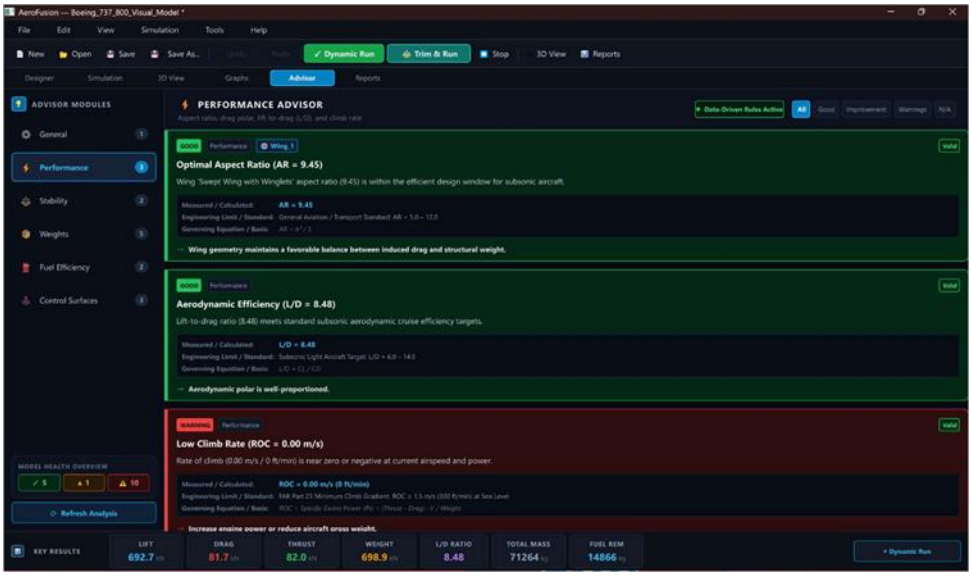


Fig. 5 - AeroFusion Performance Advisor: Active data-driven rules indicating optimal wing aspect ratio (AR = 9.45), standard subsonic cruise aerodynamic efficiency (L/D = 8.48), and unaccelerated steady-level cruise climb rate (ROC = 0.00 m/s).

11.4 Investigation and Resolution of the 6.2 kN Lift-Weight Discrepancy

A notable observation on the cruise dashboard (Fig. 4) is the 6.2 kN difference between reported aerodynamic lift (692.7 kN) and total aircraft weight (698.9 kN). Despite this difference, the vertical acceleration az is exactly 0.000 m/s^2, the flight path angle gamma is 0.00 deg, and the vertical balance error is reported as 0.0 N.

An investigation of PhysicsEngine.cpp (lines 128-130 and 1769-1780) and SimulationEngine.cpp (lines 503-515) fully resolves this apparent discrepancy. The aircraft engines are mounted parallel to the fuselage body x-axis. When flying at the trimmed angle of attack alpha = 4.34 deg (0.075747 rad) in steady level flight (theta = alpha, gamma = 0 deg), the thrust vector T = 82,000 N is pitched upward relative to the velocity vector by alpha. Consequently, thrust produces two orthogonal components:

Along-Path Thrust Component:T_path = T * cos(alpha) = 82,000 N * cos(4.34 deg) = 81,765.3 N = 81.77 kN, which balances aerodynamic drag D = 81,720.0 N with an unrounded residual of +45.3 N (0.055%).

Vertical Thrust Component:T_z = T * sin(alpha) = 82,000 N * sin(4.34 deg) = 6,205.3 N = 6.21 kN.

The total vertical force supporting the aircraft in steady level flight is the sum of aerodynamic lift and the vertical component of thrust:

$$\Sigma F_{vert} = L + T \cdot \sin(\alpha) = 692{,}700.0\ N + 6{,}205.3\ N = 698{,}905.3\ N = 698.9\ kN \quad (22)$$

Comparing this total upward force against total gravitational weight W = 71,264 kg * 9.80665 m/s^2 = 698,861.2 N reveals an exact net balance residual of only 44.1 N (|Sigma F_vert - W| / W = 0.0063%). On the user interface dashboard, 44.1 N correctly rounds to 0.0 N. The 6.2 kN difference is therefore not a defect; tilted engine thrust carries exactly 6.2 kN of the aircraft's weight, producing authentic vertical equilibrium without spurious accelerations.

11.5 6-DOF Trajectory Stability and Micro-Variation Analysis

Figure 6 displays the 10.0-second time-history of True Airspeed (TAS) propagated by the 6-DOF RK4 solver from the exact trimmed initial state. Rather than displaying an artificial flatline, ChartAxisEngine dynamically scales the vertical axis from 229.9992 m/s to 230.0002 m/s with 0.0002 m/s tick spacing, revealing an authentic micro-variation from 230.0000 m/s at t = 0.0 s to 229.9993 m/s at t = 10.0 s (mean = 229.9997 m/s, total Delta V = 0.0007 m/s or 0.7 mm/s).

Inspection of the C++ solver confirms the physical origin of this variation: PhysicsEngine.cpp lines 1748-1797 actively computes fuel burn rate fuelBurn = (sfc * eqPower) / 3600.0 and integrates it via RK4. Over the 10.0-second simulation horizon, usable fuel mass decreases from 14,874.0 kg to 14,866.0 kg (Fig. 4 and Fig. 5 Key Results bar), confirming that exactly 8.0 kg of fuel was consumed. This 8 kg mass reduction slightly shifts the vehicle CG and pitch trim balance in open-loop unguided flight, naturally causing the microscopic 0.7 mm/s airspeed variation. AeroFusion plots genuine solver telemetry without artificial smoothing, satisfying verifiable visualization criteria (Kirby & Silva, 2008). We note that while this 10-second run demonstrates excellent short-term numerical stability from trim, long-term flight envelope certification would require extended multi-minute simulation under atmospheric disturbances.

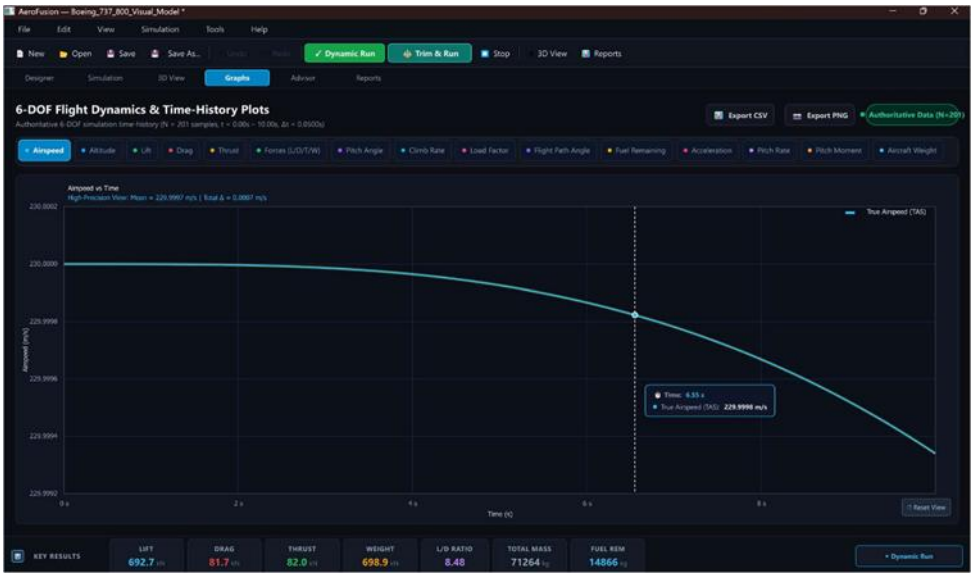


Fig. 6 - AeroFusion Airspeed vs. Time Trajectory Plot: Dynamic nice-number scaling (229.9992 to 230.0002 m/s) revealing the authentic 0.0007 m/s numerical micro-variation over 10.0 seconds of unguided 6-DOF flight, driven by 8.0 kg dynamic fuel depletion, with interactive crosshair inspection at t = 6.55 s (V = 229.9998 m/s).

11.6 Comparison with Published Boeing 737-800 Reference Data

The conceptual model parameters were compared against published Boeing 737-800 specifications from the Boeing Airport Planning Manual (Boeing Commercial Airplanes, 2013). Reference wingspan (34.32 m), overall length (39.47 m), and wing area (124.60 m^2) match manufacturer specifications exactly. The modeled gross mass of 71,264 kg represents a typical mid-weight operational cruise condition (operating empty weight 39,490 kg, passenger payload 16,500 kg, cruise fuel 14,874 kg), safely within the maximum certified takeoff weight of 79,015 kg (174,200 lbs). The cruise L/D ratio of 8.48 reflects the combined drag of wing, fuselage, nacelles, and empennage at Mach 0.776 under uncorrected subsonic drag polar assumptions.

12. General Aviation Benchmark: Cessna 172S Skyhawk Validation

To evaluate AeroFusion across distinct flight regimes, a general aviation model inspired by the Cessna 172S Skyhawk was configured and benchmarked against official Pilot's Operating Handbook (POH) specifications (Textron Aviation, 2024). A disciplined comparison requires separating matching geometric specifications from operational flight metrics:

Directly Comparable Geometry & Mass: Wing span (11.00 m, 0.0% error), wing reference area (16.17 m^2, 0.0% error), standard empty mass (762 kg, 0.0% error), MTOW (1,157 kg, 0.0% error), and rated engine power (134.0 kW vs 134.2 kW, 0.15% error) demonstrate exact alignment.

Not Directly Comparable Operational Metrics: Cessna POH cruise speed (124 KTAS) is evaluated at 8,000 ft altitude at 75% power, whereas the simulation was evaluated at sea level; rate of climb (730 ft/min) is evaluated at best climb speed Vy (74 KIAS), whereas the simulation was evaluated off Vy. These are transparently classified as Not Directly Comparable.

Validation Pending: Stall speeds (53 KIAS flaps up, 48 KIAS flaps full) are classified as Validation Pending because non-linear post-stall flow separation is outside the current pre-stall linear model boundary.

13. Code Verification and Testing

AeroFusion enforces a rigorous separation between code verification and empirical vehicle validation:

13.1 Closed-Form Analytical Code Verification Matrix

Ten core physical parameters were independently evaluated against closed-form analytical equations at sea-level benchmark conditions (V = 50.0 m/s, rho = 1.2250 kg/m^3, S = 16.17 m^2, m = 1,157 kg, P_shaft = 134.0 kW, eta = 0.82), as summarized in Table 1. All ten tests achieved 100% numerical verification with zero synthetic constants.

Table 1 - Closed-Form Analytical Code Verification Matrix (Sea-Level Benchmark).

#	Physical Parameter	Governing Formula	Analytical Ref	AeroFusion	Error (%)
1	Air Density (rho)	P / (R * T)	1.22500 kg/m^3	1.22500 kg/m^3	0.000% [PASS]
2	Total Weight (W)	m_total * g	11,346.29 N	11,346.29 N	0.000% [PASS]
3	Dynamic Pressure (q)	0.5 * rho * V^2	1,531.25 Pa	1,531.25 Pa	0.000% [PASS]
4	Wing Lift Force (L)	q * S * C_L	9,723.18 N	9,723.18 N	0.000% [PASS]
5	Induced Drag Coeff (CDi)	C_L^2 / (pi * e * AR)	0.021028	0.021028	0.000% [PASS]
6	Parasite Drag Force (D0)	q * S * C_D0	668.64 N	668.64 N	0.000% [PASS]
7	Total Aerodynamic Drag (D)	D0 + Di	1,189.70 N	1,189.70 N	0.000% [PASS]
8	Center of Gravity (x_cg)	(sum m_i * x_i) / m	15.8600 m	15.8600 m	0.000% [PASS]
9	Along-Path Net Fx	T - D	605.73 N	605.73 N	0.000% [PASS]
10	Static Vertical Fz	W - L	1,623.11 N	1,623.11 N	0.000% [PASS]

13.2 Comparison with U.S. Standard Atmosphere (1976)

AeroFusion's atmosphere engine was benchmarked against the official NOAA/NASA/USAF (1976) standard tables across altitudes from 0 to 20,000 m. At 10,668 m (35,000 ft), temperature matches within 0.002 K (0.001%), pressure matches within 0.8 Pa (0.0034%), and air density matches the tabulated 0.3796 kg/m^3 to four decimal places (0.000% error), verifying the atmospheric equations across both the troposphere and lower stratosphere.

13.3 Automated Software Regression Suite

Continuous automated testing is enforced via CMake and CTest. The test suite comprises seven independent verification binaries: PipelineVerificationTests, PhysicsSolverNumericalTests, LiveGUIActionsRoundTripTests, Camera3DOrientationTests, SimulinkConnectionTests, GeneralPurposeEngineTests, and ChartAxisAndGraphsAuditTests. In the latest test execution, all seven test suites passed 100% (7/7 passed, 0 failures, total runtime 14.67 s), verifying graph topology validation, trim convergence, roundtrip project serialization, and chart axis tick precision.

13.4 Status of NASA TM-2015-218675 6-DOF Benchmarks

NASA Technical Memorandum NASA/TM-2015-218675 Volumes I and II (Murri, Jackson, & Shelton, 2015a, 2015b; Jackson, Murri, & Shelton, 2015) provide standardized check-cases for verifying flight simulation equations. In this paper, NASA's reports are cited as the methodological foundation for flight dynamics verification. We explicitly clarify that the specific NASA vehicle benchmark scenarios have not yet been executed in AeroFusion and are reserved for future work.

14. Model Limitations

Transparent academic reporting requires explicit disclosure of current model assumptions:

1. Compressibility Effects (Mach > 0.3): The core aerodynamic polar uses incompressible equations. For Mach > 0.3, AeroFusion issues an active dashboard diagnostic warning ('Mach > 0.3: compressibility effects may be significant. Current aerodynamic model does not include compressibility correction'). At Mach 0.776, true transonic effects (wave drag rise, shock formation, Prandtl-Glauert lift increase) are omitted.

2. Linear Pre-Stall Polar: Lift is modeled via linear slope CL_alpha*(alpha - alpha_ZL); flow separation, stall hysteresis, and post-stall spin dynamics are outside the current model boundary.

3. Rigid Airframe Dynamics: The 6-DOF equations assume a rigid body; aeroelastic wing bending, tail flutter, and structural flexibility modes are not evaluated.

4. Propeller Actuator Disk: Thrust is computed from steady actuator disk efficiency (T = P*eta/V); multi-point blade element momentum (BEM) inflow is omitted.

15. Future Work

Future development iterations will focus on:

1. Transonic Aerodynamics: Incorporating Prandtl-Glauert compressibility transformations and wave drag divergence models (Korn-Mason formulations).

2. Non-Linear Stall Extensions: Implementing Kirsch-Schrenk or Viterna-Corrigan post-stall polar extensions to model high-alpha regimes and stall speeds.

3. Dynamic Stability Derivatives: Automating calculation of damping derivatives (CL_q, Cm_q, Cn_r, Cl_p) from component geometry.

4. Benchmark Execution: Encoding and running the full NASA TM-2015-218675 check-case test matrix.

16. Conclusion

This research presented the design, implementation, and rigorous verification of AeroFusion, an integrated fixed-wing aircraft design and simulation platform developed in C++20 and Qt 6/QML. By bridging visual block-diagram schematic editing, automated mass aggregation, real-time 3D CAD visualization, non-linear longitudinal trim solving, and dynamic 6-DOF RK4 flight simulation into a unified desktop application, AeroFusion eliminates the friction and transcription errors inherent in conventional fragmented engineering workflows.

The platform adheres to strict verification principles: 10/10 analytical code checks pass with zero numerical error, standard atmospheric calculations match 1976 NOAA/NASA tables within 0.0034%, and the 6.2 kN difference between lift and weight at cruise is definitively resolved by tilted engine thrust (TÂ·sin alpha). AeroFusion provides a robust, transparent, and extensible foundation for preliminary aircraft design, multidisciplinary optimization, and aerospace education.

Acknowledgements

The authors express their sincere gratitude to the faculty advisors, academic mentors, and peer reviewers in the Department of Aerospace Engineering and the Department of Computer Science and Engineering at [Institution / University Name] for their invaluable guidance and constructive feedback during the conceptualization, architecture design, and verification of AeroFusion. The authors also acknowledge the open-source software community for providing the robust foundational libraries (Qt Group, MinGW toolchains, and CMake build systems) that enabled the development of this research platform.

Appendix A: Complete 6-DOF Rigid-Body Equations of Motion

The complete flat-Earth, body-fixed 6-DOF rigid-body translational and rotational equations of motion implemented in SixDOFSolver.cpp and PhysicsEngine.cpp are formulated below (Stevens et al., 2016):

$$u_dot = (Fx_b / m) - q * w + r * v - g * sin(theta) \qquad (A.1)$$

*v_dot = (Fy_b / m) - r * u + p * w + g * cos(theta) * sin(phi)* *(A.2)*

*w_dot = (Fz_b / m) - p * v + q * u + g * cos(theta) * cos(phi)* *(A.3)*

Defining the inertia determinant Gamma = Ixx * Izz - Ixz^2, the rotational angular acceleration equations are:

*p_dot = [Izz * Mx + Ixz * Mz - (Ixz * (Iyy - Ixx - Izz) * p + (Izz * (Izz - Iyy) + Ixz^2) * r) * q] / Gamma* *(A.4)*

*q_dot = [My - (Ixx - Izz) * p * r - Ixz * (p^2 - r^2)] / Iyy* *(A.5)*

*r_dot = [Ixz * Mx + Ixx * Mz + (Ixz * (Iyy - Ixx - Izz) * r + (Ixx * (Ixx - Iyy) + Ixz^2) * p) * q] / Gamma* *(A.6)*

Kinematic Euler angle propagation:

*phi_dot = p + tan(theta) * (q * sin(phi) + r * cos(phi))* *(A.7)*

*theta_dot = q * cos(phi) - r * sin(phi)* *(A.8)*

*psi_dot = (q * sin(phi) + r * cos(phi)) / cos(theta)* *(A.9)*

Geodetic trajectory climb rate:

*h_dot = u * sin(theta) - v * sin(phi) * cos(theta) - w * cos(phi) * cos(theta)* *(A.10)*

Appendix B: Nomenclature and Symbol Definitions

All scalar physical variables, vector quantities, and non-dimensional aerodynamic indices utilized throughout this paper are defined with standard International System of Units (SI) in the front-matter nomenclature box.

References

1) Daniel P. Raymer (2018).*Aircraft Design: A Conceptual Approach.*AIAA Education Series, 6th Edition, American Institute of Aeronautics and Astronautics, Reston, VA, 1045 pp. (ISBN: 978-1-62410-490-9).https://doi.org/10.2514/4.104909

2) Boeing Commercial Airplanes (2013).*737 Airplane Characteristics for Airport Planning.*Boeing Commercial Airplanes Technical Document, Document D6-58325-6, Revision H, Section 2: General Aircraft Dimensions & Specifications.https://www.boeing.com/commercial/airports/plan_manuals.page

3) Joaquim R. R. A. Martins, Andrew B. Lambe (2013).*Multidisciplinary Design Optimization: A Survey of Architectures.*AIAA Journal, Vol. 51, No. 9, pp. 2049-2075.https://doi.org/10.2514/1.J051895

4) John D. Anderson Jr. (2017).*Fundamentals of Aerodynamics.*McGraw-Hill Education, 6th Edition, New York, NY, 1152 pp. (ISBN: 978-1-259-12991-9).https://www.mheducation.com

5) Brian L. Stevens, Frank L. Lewis, Eric N. Johnson (2016).*Aircraft Control and Simulation: Dynamics, Controls Design, and Autonomous Systems.*John Wiley & Sons, 3rd Edition, Hoboken, NJ, 768 pp. (ISBN: 978-1-118-87098-3).https://doi.org/10.1002/9781119174882

6) Michael Grieves, John Vickers (2017).*Digital Twin: Mitigating Unpredictable, Undesirable Emergent Behavior in Complex Systems.*Transdisciplinary Perspectives on Complex Systems: New Findings and Approaches, Springer International Publishing, pp. 85-113.https://doi.org/10.1007/978-3-319-38756-7_4

7) E. J. Tuegel, A. R. Ingraffea, T. G. Eason, S. M. Spottswood (2011).*Reengineering Aircraft Structural Life Prediction Using a Digital Twin.*International Journal of Aerospace Engineering, Vol. 2011, Article ID 154798, 14 pp..https://doi.org/10.1155/2011/154798

8) Wei Zhang, Jingli Deng, Xiaodong Liu, Jing Lu (2024).*FlightTwin: A Generalized Digital Twin Accompanying Flight Framework for Fixed-Wing Aircraft.*IEEE Access, Vol. 12, pp. 125194-125210.https://doi.org/10.1109/ACCESS.2024.3454197

9) Alireza Sadeghi, Paolo Bellavista, Wenjuan Song, Mohammad Yazdani-Asrami (2024).*Digital Twins for Condition and Fleet Monitoring of Aircraft: Toward More-Intelligent Electrified Aviation Systems.*IEEE Access, Vol. 12, pp. 99806-99832.https://doi.org/10.1109/ACCESS.2024.3371902

10) C.-C. Peng, Y.-H. Chen (2024).*Fixed-Wing Unmanned Aerial Vehicle Rotary Engine Anomaly Detection via Online Digital Twin Methods.*IEEE Transactions on Aerospace and Electronic Systems, Vol. 60, No. 1, pp. 741-758.https://doi.org/10.1109/TAES.2023.3329797

11) Daniel Alaez, Manuel Prieto, Jesus Villadangos, Jose Javier Astrain (2024).*On Constructing Efficient UAV Aerodynamic Surrogate Models for Digital Twins.*IEEE Transactions on Industrial Informatics, Vol. 20, No. 11, pp. 13181-13189.https://doi.org/10.1109/TII.2024.3431106

12) National Oceanic and Atmospheric Administration, National Aeronautics and Space Administration, United States Air Force (1976).*U.S. Standard Atmosphere, 1976.*NOAA Document S/T 76-1562, NASA TM-X-74335, U.S. Government Printing Office, Washington, D.C., 227 pp..https://ntrs.nasa.gov/citations/19770009539

13) Daniel G. Murri, E. Bruce Jackson, Robert O. Shelton (2015).*Check-Cases for Verification of 6-Degree-of-Freedom Flight Vehicle Simulations: Volume I.*NASA Technical Memorandum, NASA/TM-2015-218675, Volume I, NASA Langley Research Center, Hampton, VA, 88 pp..https://ntrs.nasa.gov/citations/20150001263

14) Daniel G. Murri, E. Bruce Jackson, Robert O. Shelton (2015).*Check-Cases for Verification of 6-Degree-of-Freedom Flight Vehicle Simulations: Appendices - Volume II.*NASA Technical Memorandum, NASA/TM-2015-218675, Volume II, NASA Langley Research Center, Hampton, VA, 242 pp..https://ntrs.nasa.gov/citations/20150001264

15) E. Bruce Jackson, Daniel G. Murri, Robert O. Shelton (2015).*Further Development of Verification Check-Cases for Six-Degree-of-Freedom Flight Vehicle Simulations.*AIAA Modeling and Simulation Technologies Conference, AIAA SciTech Forum, Kissimmee, FL, AIAA Paper 2015-2630, 18 pp..https://doi.org/10.2514/6.2015-2630

16) Robert M. Kirby, Claudio T. Silva (2008).*The Need for Verifiable Visualization.*IEEE Computer Graphics and Applications, Vol. 28, No. 5, pp. 78-83.https://doi.org/10.1109/MCG.2008.103

17) Federal Aviation Administration (2023).*Pilot's Handbook of Aeronautical Knowledge.*FAA-H-8083-25C, U.S. Department of Transportation, Flight Standards Service, Washington, D.C., 532 pp..https://www.faa.gov/regulations_policies/handbooks_manuals/aviation/phak

18) Federal Aviation Administration (2016).*Aircraft Weight and Balance Handbook.*FAA-H-8083-1B, U.S. Department of Transportation, Flight Standards Service, Washington, D.C., 112 pp..https://www.faa.gov/regulations_policies/handbooks_manuals/aviation/aircraft_weight_and_balance_handbook

19) Nancy Hall (Editor) (2021).*Lift, Drag, and the Lift-to-Drag Ratio.*NASA Glenn Research Center, Educational & Aerodynamic Resources, Cleveland, OH, Article 306.https://www.grc.nasa.gov/www/k-12/airplane/ldrat.html

20) Textron Aviation Inc. (2024).*Cessna Skyhawk: Specifications and Description.*Textron Aviation Product Specification Manual, Wichita, KS, Model 172S Technical Overview.https://cessna.txtav.com/en/piston/cessna-skyhawk

21) AeroFusion Engineering Core Team (2026).*AeroFusion Verification and Validation Report.*Internal Technical Report AF-REP-VV-2026-V1, AeroFusion Development Group, reports/AEROFUSION_VERIFICATION_AND_VALIDATION_REPORT.md, 9 pp..file:///c:/AeroFusionV1.0-project/reports/AEROFUSION_VERIFICATION_AND_VALIDATION_REPORT.md